

Structure and reactions of ^{11}Be : many-body basis for single-neutron halo

F. Barranco,¹ G. Potel,² R.A. Broglia,^{3,4} and E. Vigezzi⁵

¹*Departamento de Física Aplicada III, Escuela Superior de Ingenieros, Universidad de Sevilla, Camino de los Descubrimientos, Sevilla, Spain*

²*National Superconducting Cyclotron Laboratory, Michigan State University, East Lansing, Michigan 48824, USA*

³*The Niels Bohr Institute, University of Copenhagen, DK-2100 Copenhagen, Denmark*

⁴*Dipartimento di Fisica, Università degli Studi Milano, Via Celoria 16, I-20133 Milano, Italy*

⁵*INFN Sezione di Milano, Via Celoria 16, I-20133 Milano, Italy*

The exotic nucleus ^{11}Be has been extensively studied and much experimental information is available on the structure of this system. Treating, within the framework of empirically renormalised nuclear field theory (NFT)_{ren} in both configuration and 3D-space, the mixing of bound and continuum single-particle (sp) states through the coupling to collective particle-hole (p,h) and pairing vibrations of the ^{10}Be core, as well as Pauli principle acting not only between the particles explicitly considered and those participating in the collective states, but also between fermions involved in two-phonon virtual states it is possible, for the first time, to simultaneously and quantitatively account for the energies of the $1/2^+$, $1/2^-$ low-lying states, the centroid and line shape of the $5/2^+$ resonance, the one-nucleon stripping and pickup absolute differential cross sections involving ^{11}Be as either target or residual nucleus, and the dipole transitions connecting the $1/2^+$ and $1/2^-$ parity inverted levels as well as the charge radius, thus providing a unified and exhaustive characterisation of the many-body effects which are at the basis of this paradigmatic one-neutron halo system.

PACS numbers: 21.60.Jz, 23.40.-s, 26.30.-k

At the basis of nuclear structure, one finds the unification (A. Bohr and Mottelson) of the shell model (Mayer and Jensen) and the collective model (N. Bohr and Wheeler). One nucleon moving outside closed shell constitutes a unique laboratory to test the validity of the above picture in systems which are at the limit of stability of neutron or proton excess, drip lines being charted with inverse kinematics techniques involving rare isotope beams [1]. The neutron drip line nucleus ^{11}Be provides a rare and precious window into the virtual processes clothing neutrons which, through a rather conspicuous Lamb-shift-like effect, of the order of 10% of the value of the Fermi energy, invert parity, thus allowing for the emergence of a new magic number diverse from that of Meyer-Jensen and extending, in the process, the limits of stability of nuclear species.

Information about the nucleus ^{11}Be is available regarding the $1/2^+$, $1/2^-$ and $5/2^+$ low-lying levels, including the line shape of the $5/2^+$ resonance, in particular from inelastic and transfer reactions [2–7] (Fig. 1(exp)). Analyses of these reactions have been reported in [8–13]. Information concerning the charge radius [14] and the dipole transition between the ground state and the first excited state [15] is also available. Theoretical work on the structure of ^{11}Be has been carried out, starting from parity inversion between the $1/2^+$ and the $1/2^-$ levels, within the shell model [16], while results of studies based on the coupling of particles to vibrations and rotations are found in refs. [17]–[20] and [13, 21, 22] respectively. A static description of ^{11}Be based on a deformed mean field was presented in [23]. Results of investigations within the framework of antisymmetrized molecular dynamics were reported in [24]. The outcomes of ab initio approaches are found in [25]. Results of calculations of charge radii based on fermionic molecular dynamics have been reported in ref. [26].

In this letter we are able to achieve a unified and accurate

description of both structure and reaction aspects of ^{11}Be . To do so, one has to deal simultaneously with the $p_{3/2}$, $p_{1/2}$, $s_{1/2}$ and $d_{5/2}$ states, treating their interweaving with quadrupole and octupole (p,h) vibrations and monopole pair vibrations on equal footing, as well as to take into account the mixing between bound and continuum states. Furthermore, one has to consider the Pauli principle acting between the particle explicitly considered and those participating in the vibrations as well as between those participating in two-phonon states. Because of spatial quantization, the above requirement involves both energies and single-particle radial wave functions, in particular that of the $d_{5/2}$ resonance. The variety of many-body clothing processes lead to important modifications of these radial wave functions, and thus of the corresponding one-particle transfer form factors and escape particle wave functions, accounting for up to 50% changes in the value of the one-nucleon transfer absolute cross sections and of the $5/2^+$ resonance decay width, in overall agreement with experimental data. It will be furthermore demonstrated that crucial information concerning the nature of the $5/2^+$ resonance and the role of the quadrupole mode in dressing the nucleons moving around the Fermi surface is provided by the reactions $^{10}\text{Be}(d,p)^{11}\text{Be}(5/2^+)$, 1.833 MeV and $^{11}\text{Be}(p,d)^{10}\text{Be}(2^+)$; 3.33 MeV which forces, in this last case, a virtual state, to become observable. A fact that aside from shedding light on retardation in clothing processes, implies that particle-vibration coupled intermediate states which cloth the single-particle states have to be real, empirical states concerning both energy and amplitude, as well as radial shape. Thus, (NFT)_{ren} is not a calculational ansatz but a quantal requirement. Within this context, it is of notice that self consistency within (NFT)_{ren} implies that the final results $\tilde{\epsilon}_j^{(i)}$ and $\tilde{\phi}_j(r)^{(i)}$ reproduce the empirical input used for the intermediate states, while initial states (energies and wave functions) of the variety of graphi-

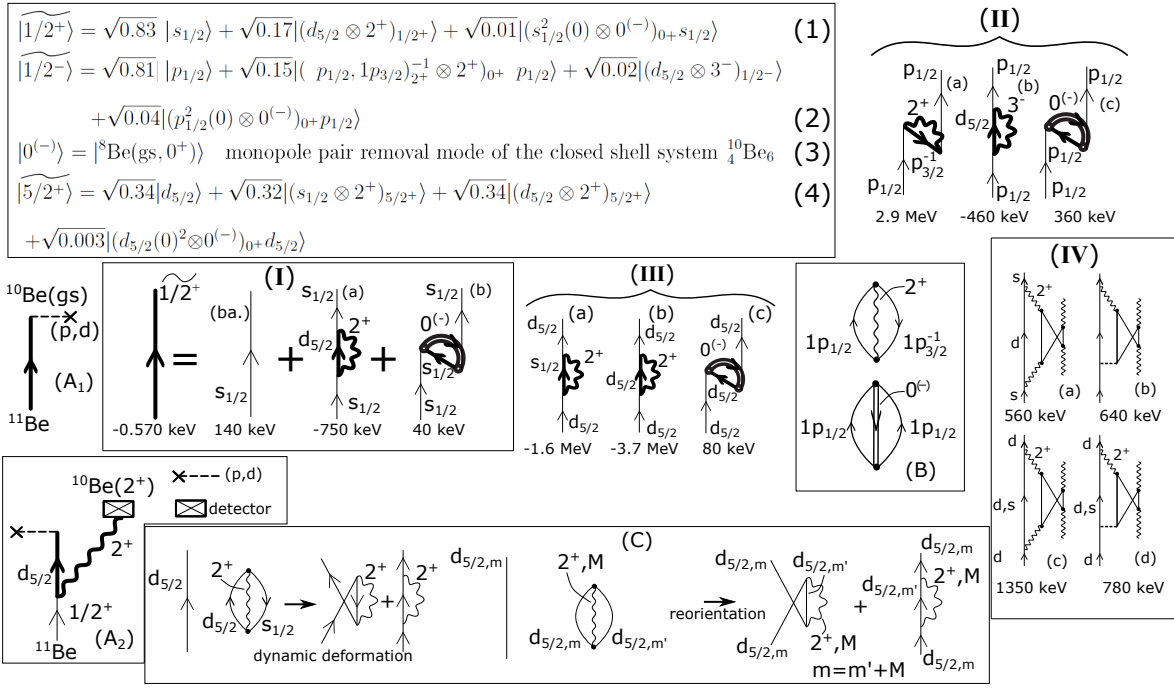


FIG. 1. (Upper box) Wavefunctions associated with the renormalised single-particle levels labeled NFT in Fig. 1. (Lower Box) NFT diagrams describing the processes responsible for the variety of components of the clothed states. Single-arrowed lines pointing up (down) describe particle (hole) states, while wavy lines represent collective particle-hole (ph)vibrational states. Double arrowed lines pointing down describe the correlated (hh) pair removal vibrational states. The dashed horizontal line describes the two-body multipole, separable interaction. In calculating the intermediate states of the diagrams displayed in I-III the experimental and/or renormalised fermions bosons modes have been used (empirical renormalisation). This is the reason why they are displayed in terms of bold face lines and curves. The diagrams shown in IV take care of the Pauli principle violation of the two phonon states appearing in these intermediate states. The label (ba.) in (I) stands for bare.

cal contributions are solutions of the bare potential. In other words, for each value of $\tilde{\epsilon}_j$ there can exist more than one radial function, depending on whether the nucleon is moving around the ground state ($i = gs$) or around an excited state of the core ($i = coll$) respectively. Technically, $\tilde{\phi}_j(r)^{(i)}$ are the form factors associated with stripping and pickup reactions around closed shells. For simplicity we will drop the superscript i in what follows.

Making use of this theoretical framework ([27] and refs. therein, see also [28, 29]) we have calculated the variety of self energy diagrams, normalizing selfconsistently the motion of the odd neutron of ${}^{11}\text{Be}$ in both configuration- (Fig. 1) and conformation 3D-space (Fig. 2). The energies $\tilde{\epsilon}_j$ of the associated renormalised single-particle states (drawn with bold face arrowed lines in Fig. 1) are shown in Fig. 3 (NFT) in comparison with the data (exp.), while the corresponding wave functions $\tilde{\phi}_j(r)$ are displayed in Fig. 2 in comparison with those corresponding to the separation energy approximation obtained by adjusting the depth of a standard Saxon-Woods potential ([36], Eq. (2-180)) so as to reproduce the separation energy of each state in question making use of an effective mass equal to the free nucleon mass. The quadrupole- and octupole - as well as monopole pair removal - vibrational modes of the core ${}^{10}\text{Be}$ (Fig. 3 inset) and associated particle vibration coupling (PVC) vertices were worked out in QRPA ($\beta_2^n = 0.9$

and $\beta_3^n = 0.28$) and in RPA respectively with the help of separable interactions of self consistent strength. They are drawn in Fig. 1 in terms of bold face wavy curves (quadrupole and octupole) and arrowed double lines (pair mode). We remark that the error in the self-energy associated with overcounting (bubble correction) in the sum over intermediate particle-phonon configurations, amounts to at most to a few percent effect in the present case (Suppl. Mat., Section 3) .

The bare states (thin arrowed lines in Fig.1) were determined as solutions of a mean field potential of radial dependent k -mass. This field was parameterized as a Saxon-Woods potential with a spatially dependent effective mass of value $m_k(0) = 0.7m$ at the center of the nucleus and $\mu = 0.91m$ (reduced mass value) far from it. The parameters were varied starting from values reproducing the shape of the mean field obtained with the SGII Skyrme interaction (Table 1; see also Suppl. Mat, Section 1). The resulting bare energies ϵ_j and wave functions ϕ_j are shown in Figs. 3 (bare) and 2 respectively.

The clothed states associated with a given quantum number result from the iterative diagonalization of the PVC Hamiltonian in a space composed of single-particle and of particle-phonon states, making use of self-energy function techniques (Fig. 1(I), see also Suppl. Mat., Section 2). We included in the calculation the $s_{1/2}$, $p_{1/2}$ and $d_{5/2}$ single-particle states up

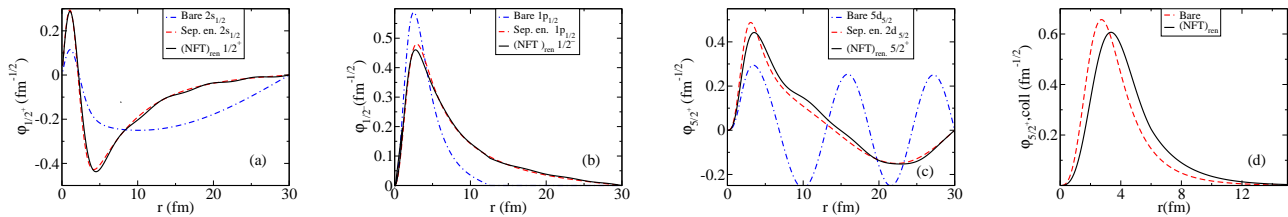


FIG. 2. The form factors of the $1/2^+$ (a), $1/2^-$ (b), $5/2^+$ (c) states and (d) the form factor associated with the reaction $^{11}\text{Be}(p,d)^{10}\text{Be}(2^+)$ calculated within the framework of NFT and empirical normalisation in a box of radius $R_{\text{box}} = 30$ fm, divided by the associated amplitudes ($a_{1/2^+} = \sqrt{0.83}$, $a_{1/2^-} = \sqrt{0.81}$, $a_{5/2^+} = \sqrt{0.34}$, $a_{(d_{5/2^+} \otimes 2^+)_{1/2^+}} = \sqrt{0.17}$, see Fig. 1, upper box) are compared to the corresponding separation energy approximation wavefunctions and to the wave functions calculated with the bare potential parameterized as reported in Table I.

to an energy $E_{\text{cut}} = 25$ MeV, imposing vanishing boundary conditions at $R = 30$ fm (continuum discretization), leading to matrices of typical dimension $N \approx 300$. The lowest $p_{3/2}$ state was also included. The diagonalization process is equivalent to the solution of a system of coupled integro-differential equations (see [35] and Suppl. mat., Section 7). The interference between the amplitudes of the various single-particle states determines the radial dependence of the single-particle component of the eigenstates, in particular in the surface region (Fig. 2).

The most conspicuous effect emerging from these NFT results is the (absolute value) reduction of the energy difference between positive and negative parity states (Fig. 3): a factor of ten in the case of $1/2^-$, $1/2^+$ states (from $\epsilon_{1/2^+} - \epsilon_{1/2^-} = +3.2$ MeV (bare) to $\bar{\epsilon}_{1/2^+} - \bar{\epsilon}_{1/2^-} = -0.3$ MeV (NFT)) and of six in the case of $5/2^+$, $1/2^-$ states (from $\epsilon_{5/2^+} - \epsilon_{1/2^-} = +9.5$ MeV (bare) to $\bar{\epsilon}_{5/2^+} - \bar{\epsilon}_{1/2^-} = +1.5$ MeV (NFT)). While parity inversion is only observed in the first case, the second had a close call, playing an essential role in the mechanism which is at the basis of $(1/2^+, 1/2^-)$ parity inversion ($1/2^+$ self energy polarisation (PO) and $1/2^-$ correlation (CO) processes [31] arising from Pauli principle of the odd neutron and ZPF of the core ground (vacuum) state). It is an open question whether parity inversion between $1/2^-$ and $5/2^+$ states can ever be observed in nuclei.

As testified by the components of the clothed states displayed in Fig. 1 (upper box), the physics at the basis of the results reported above is mainly related to the coupling of single-particle to dynamical, ω -dependent, quadrupole deformation, conspicuously modified by Pauli principle corrections. Let us start with the $5/2^+$ resonance. This state is prone to acquire a dynamical quadrupole moment (reorientation effect, see Fig. 1 inset (C)). This is because the particle-vibration coupling of the $d_{5/2^+}$ with itself through the excitation of the quadrupole vibration of ^{10}Be , involving a rather confined single-particle resonant state radial wave function (Fig. 2 (c)), results in a large value of $\langle \tilde{\psi}_{5/2^+} | R_0 dU/dr | \tilde{\psi}_{5/2^+} \rangle$ and thus in a large non spin-flip PVC matrix element

$\langle 5/2^+ \otimes 2^+ \rangle_{5/2^+} | H_c | d_{5/2} \rangle \approx -4.6$ MeV leading to an amplitude of $\sqrt{0.34}$ for the many-body state $|(d_{5/2} \otimes 2^+)_{5/2^+} \rangle$ (Fig. 1, upper box, Eq.(4)). An equally important component

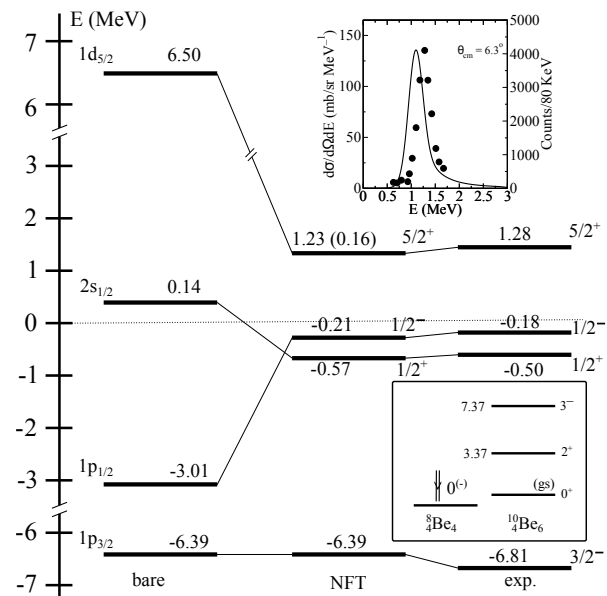


FIG. 3. Low-lying spectrum of ^{11}Be : (bare) unperturbed single-particle levels, solution of the bare mean field; (NFT) renormalised levels; (Exp.) experimental values. The number on each thick horizontal line is the energy of the state in MeV. The number in brackets correspond to the width of the $5/2^+$ resonance derived from the calculated elastic phase shifts. No phase shift data exist for this state, the 100 keV width often quoted being extracted from the $^9\text{Be}(t,p)^{11}\text{Be}(5/2^+)$ reaction ([30], Table 11.5). The line shape of the $5/2^+$ resonance is displayed in the upper rhs corner in comparison with the data. In the lower right corner inset, the collective modes employed in the clothing of the bare single-particle states (first column) are shown. The label $0^{(-)}$ indicates the correlated two-hole state, monopole ($J^\pi = 0^+$) pair removal mode.

($\approx \sqrt{0.34}$) is associated with the coupling of the $5/2^+$ state to the $s_{1/2}$ state, again through the quadrupole mode. This coupling allows the bare $d_{5/2}$ resonance ($\epsilon_{5/2^+} \approx 6.5$ MeV, Fig. 3), to explore halo-like regions of the system and to lower its kinetic energy. Together with the effects of the couplings discussed above and the repulsive one associated with the coupling to the pair removal mode, it results in an overall energy decrease of the $5/2^+$ strength and in the buildup of a narrow (Fig. 3 inset line shape) resonance with centroid at $E = 1.23$

MeV and a width of 160 keV calculated from elastic scattering phase shifts (Suppl. Mat., Sect. 2). In turn, the $2s_{1/2}$ wave function mixes with the $(d_{5/2} \otimes 2^+)$ configuration and acquires a component of sizable amplitude ($\approx \sqrt{0.17}$) lowering, in the process, its energy by about 750 keV (Fig. 1 (I)(a)), the repulsion due to Pauli principle and arising from the mixing with the $(s_{1/2} \otimes 0^{(-)})$ configuration being rather modest (Fig. 1 (I(b))). In other words, the $5/2^+$ state plays, through its coupling to the 2^+ vibration of the core, an essential role in the $(1/2^-, 1/2^+)$ parity inversion phenomenon.

The zero-point fluctuations (ZPF) associated with the ^{10}Be core, both those arising from the quadrupole vibrations as well as from the monopole pair removal mode (boxed inset (B) of Fig. 1) make virtual use of the $p_{1/2}$ single-particle state. The first and third NFT diagrams displayed in Fig. 1 (II) properly treat the problem of the identity of the particles appearing explicitly and the particles participating in the collective motion. As a result, the phase space of the clothed $1p_{1/2}$ state becomes smaller than the bare one, its binding becoming weaker by about 3 MeV due to the Lamb-shift-like process shown in Fig. 1 (II)(a) and by 360 keV due to that displayed in Fig. 1(II)(c), the contribution of the second graph (Fig. 1 (II)(b)) being attractive. The numbers quoted above contain, among other things, the renormalisation contribution of the Pauli correcting diagrams shown in Fig. 1 (inset(IV) right hand side) and associated with the implicit presence of two-phonon states in intermediate, virtual configurations, drawn in bold face.

The radial dependence of the many-body wavefunctions and the phonon admixture can be probed by the one-neutron transfer reactions $^{10}\text{Be}(d,p)^{11}\text{Be}$ and $^{11}\text{Be}(p,d)^{10}\text{Be}(2^+)$, populating the low-lying $1/2^+$, $1/2^-$ and $5/2^+$ states of ^{11}Be and the first excited 2^+ state of ^{10}Be , and proceeding through the form factors displayed in Figs. 2(a)-(c) and Fig. 2(d) respectively. Concerning the latter, we remark that the asymptotic decay constant of the $d_{5/2}$ radial wave function associated with the $2^+ \otimes d_{5/2}$ configuration admixed in the $1/2^+$ ground state of ^{11}Be displays a binding energy $\tilde{\epsilon}_{1/2^+} - \hbar\omega_{2^+} = -3.8$ MeV. It is a natural outcome of $(\text{NFT})_{ren}$ to give rise, through PVC and Pauli mechanism, to the proper clothing of the $d_{5/2}$ orbital so as to be able "to exist" inside the $|s_{1/2}\rangle$ state as a virtual, intermediate configuration (Fig. 1(I)(a) and IV(a) and (b)). The associated asymptotic r -behaviour results from the coherent superposition of many continuum states, and its spatial dependence in the surface region (Fig. 2 (d)) can hardly be simulated by making use of a bound single-particle wavefunction of a properly parameterized single-particle potential (separation energy approximation), in agreement with the result of previous studies [4].

The $(\text{NFT})_{ren}$ form factors shown in Fig. 2 were used, together with global optical potentials [32, 33], to calculate the one-nucleon stripping and pickup absolute differential cross sections of the reactions mentioned above. The results provide an overall account of the experimental findings (Fig. 4). Within this context we remark that the pickup process shown in inset (A₁) of Fig. 1 and populating ^{10}Be ground state implies the action of the external (p,d) field on the left hand side

(lhs) of the graphical representation of Dyson equation shown in Fig. 1(I), and involves, at the same time, the use of the corresponding radial wavefunction as formfactor (Fig. 2(a)). In the case of the population of the first 2^+ excited state of ^{10}Be (inset A₂), the (p,d) field acts on the $(d_{5/2} \otimes 2^+)_{1/2^+}$ virtual state of the second graph of the right hand side (rhs) of this equation (Fig. 1(I)(a)), involving this time the form factor shown in Fig. 2(d). Summing up, insets (A₁) and (A₂) and diagrams (I) of Fig. 1 testify to the subtle effects resulting from the unification of $(\text{NFT})_{ren}$ of structure and reactions discussed in [27], and operative in the cross sections shown in Fig. 4, as a result of the simultaneous and self consistent treatment of configuration and 3D-space. Within this context the bold face drawn state $|d_{5/2} \otimes 2^+_{1/2^+}\rangle$ shown in Fig. 1(I)(a) and the wave function displayed in Fig. 2(d) can be viewed as *on par* structure and reaction intermediate elements of the quantal process $^{11}\text{Be}(1/2^+)(p,d)^{10}\text{Be}(2^+)$.

Particle-vibration coupling leads to important renormalization effects in the radius and in the dipole electromagnetic transitions of the system, the two phenomena being closely related. This is due to the poor overlap between the resulting renormalised halo radial wave functions and those of the core nucleons which screen the symmetry potential, impeding the GDR to shift the $1/2^+ \rightarrow 1/2^-$ single-particle E1-strength to high energies in the attempt to exhaust the EWSR [23, 27, 34].

The strength of the dipole transition connecting the ground and the first excited states was calculated and compared to the experimental value $B(E1) = 0.102 \pm 0.002 e^2 \text{ fm}^2$. Estimates carried out using single-particle wavefunctions corresponding to the separation energy approximation and normalised to one, give $B(E1; I_i \rightarrow I_f) = \frac{e_{eff}^2 |\langle I_f || iM(E1) || I_i \rangle|^2}{2\pi 2I_i+1} = 0.29 e^2 \text{ fm}^2$, with $e_{eff} = 4/11$. Including the renormalizations associated with the phonon admixture of the $1/2^+$ and $1/2^-$ state leads to $B(E1; 1/2^- \rightarrow 1/2^+) = 0.11 e^2 \text{ fm}^2$, that is to a reduction of over a factor of 2 bringing theory in overall agreement with the data (cf. Suppl. Mat., Section 5).

V (MeV)	V_s (MeV)	a (fm)	R (fm)
70	14	0.81	2.10

TABLE I. Optimal values of the depth, radius, diffuseness and spin-orbit strength of the bare mean field potential V, V_s, a, R (see [36] Eq. (2-180)).

Let us now discuss the isotopic shift of the charge radius (Suppl. Mat., Section 6). The corrections to the charge mean square radius $\langle r^2 \rangle_{^{10}\text{Be}}$ arising from the addition of a neutron are obtained applying the external field operator r^2 to the different particle and collective vibration lines and curves of the diagrams appearing in the rhs of the graphical equation displayed in Fig. 1(I). The summed (recoil) contributions associated with the $s_{1/2}$ state (graphs (b) and (a)) $(\langle r^2 \rangle_{1/2^+}^{1/2} / 11)^2 (\langle r^2 \rangle_{1/2^+}^{1/2} = 7 \text{ fm})$ is to be multiplied by the square of the renormalised $|1/2^+\rangle$ state single-particle ampli-

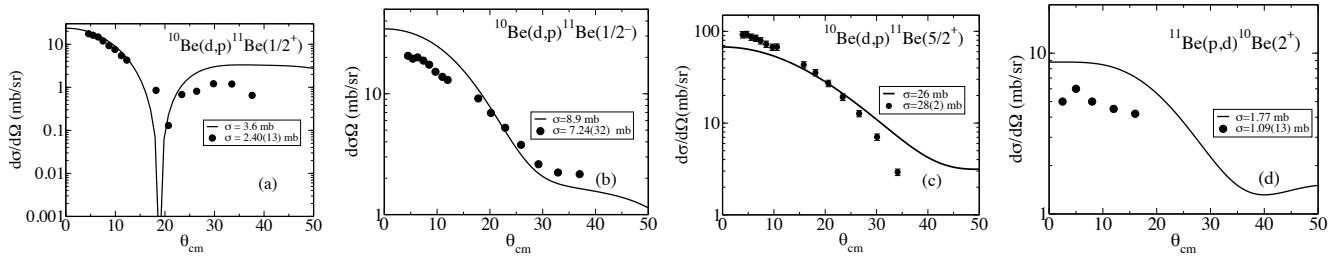


FIG. 4. (a-c) (continuous curve) Absolute differential and summed cross sections associated with the reactions $^{10}\text{Be}(d,p)^{11}\text{Be}$, populating the $1/2^+$, $1/2^-$, and $5/2^+$ states ($E_d = 21$ MeV). The experimental data [7] are displayed in terms of solid dots. (d) Same as before, but for the reaction $^{11}\text{Be}(p,d)^{10}\text{Be}$, populating the 2^+ state ($E_p = 35.3$ MeV/n) [4].

tude ($=0.83$, Fig. 1(1), upper box). Those associated with the $d_{5/2}$ and 2^+ elementary modes appearing in the intermediate state of graph (a) of Fig. 1(I) lead to (recoil) ($\langle r^2 \rangle_{5/2^+}^{1/2} / 11$)² and (dynamical deformation) ($\langle r^2 \rangle_{5/2^+}^+ \beta_{5/2}^2 / 2\pi$) contributions respectively, and are to be multiplied by the square amplitude ($=0.17$) associated with the $(d_{5/2} \otimes 2^+)_{1/2^+}$ configuration (Fig. 1, upper box). Contributions arising from graph (b) of Fig. 1(I) are not considered in keeping with their small relative values. The resulting theoretical prediction $\langle r^2 \rangle_{^{11}\text{Be}}^{1/2} = 2.48$ fm, accurately reproduces the experimental finding 2.44 ± 0.06 fm.

We conclude that a consistent fraction of the clothed one-neutron halo valence single-particle states $|j\rangle$ of ^{11}Be , as much as 60% in the case of the $|5/2^+\rangle$ state, corresponds to many-body configurations resulting from Pauli principle and particle-vibration coupling effects. These components, which modify both the single-particle content and the radial dependence of the associated wave functions, play a central role in providing an overall quantitative account of an essentially "complete" set of data characterising the structure of ^{11}Be . The existence of a bare potential, empirically determined (minimisation procedure) as an appropriate basis for nuclear many-body studies, can be considered as a benchmark of mean field theories.

Acknowledgment

F.B and E.V. acknowledge funding from the European Union Horizon 2020 research and innovation program under Grant Agreement No. 654002.

[1] I. Tanihata and R. Kanungo, Prog. Part. Nucl. Phys. **68** (2013) 215
 [2] H. Iwasaki et al., Phys. Lett. B **481** (2000) 7
 [3] S. Fortier et al., Phys. Lett. B **461** (1999) 22
 [4] J.S. Winfield et al., Nucl. Phys. A **683** 48 (2001)
 [5] D.L. Auton, Nucl. Phys. A **157**, 305 (1970)
 [6] B. Zwieglinski et al., Nucl. Phys. A **315**, 124 (1979)
 [7] K.T. Schmitt et al., Phys. Rev. C **88** (2013) 064612 Phys. Rev. C **79** (2009) 014302

[8] N.R. Timofeyuk and R.C. Johnson, Phys. Rev. C **59** (1999) 1545
 [9] N. Keeley, N. Alamanos and V. Lapoux, Phys. Rev. C **69** (2004) 064604
 [10] A. Deltuva, Phys. Rev. C **79** (2009) 054603
 [11] A. Deltuva, Phys. Rev. C **88** (2013) 011601(R)
 [12] J.A. Lay, A.M. Moro, J.M. Arias and Y. Kanada-En'yo, Phys. Rev. C **89** (2014) 014333
 [13] R. de Diego, J.M. Arias, J.A. Lay, A.M. Moro, Phys. Rev. C **89** (2014) 064609
 [14] W. Nörtershäuser et al, Phys. Rev. Lett. **102** (2009) 062503
 [15] E. Kwan et al., Phys. Lett. B **732** (2014) 210
 [16] I. Talmi and I. Unna, Phys. Rev. Lett. **4**, 469 (1960)
 [17] T. Otsuka, N. Fukunishi, and H. Sagawa, Phys. Rev. Lett. **70** (1993) 1385
 [18] H. Sagawa, B. A. Brown, and H. Esbensen, Phys. Lett. B **309** (1993) 1
 [19] N. Vinh Mau, Nucl. Phys. A **592** (1955) 33
 [20] G. Gori, F. Barranco, E. Vigezzi and R.A. Broglia, Phys. Rev. C **69** (2004) 041302(R)
 [21] F.M. Nunes, I.J. Thompson and R.C. Johnson, Nucl. Phys. A **596** (1996) 171
 [22] K. Fossez, W. Nazarewicz, Y. Jaganathen, N. Michel, and M. Ploszajczak, Phys. Rev. C **93** (2016) 011305(R)
 [23] I. Hamamoto and S. Shimoura, J. Phys. G **34** (2007) 2715
 [24] Y. Kanada-En'yo and H. Horiuchi, Phys. Rev. C **66** (2002) 024305
 [25] A. Calci, P. Navrátil, R. Roth, J. Dohet-Eraly, S. Quaglioni and G. Hupin, Phys. Rev. Lett. **117** (2016) 242501
 [26] A. Krieger et al., Phys. Rev. Lett. **108** (2012) 142501
 [27] R.A. Broglia, P.F. Bortignon, F. Barranco, E. Vigezzi, A. Idini and G. Potel, Phys. Scr. **91** (2016) 063012
 [28] R.D. Mattuck, A guide to Feynman diagrams in the many-body problem, Dover, New York (1976)
 [29] A. Idini, G. Potel, F. Barranco, E. Vigezzi and R.A. Broglia, Phys. Rev. C **92** (2015) 014331
 [30] J.H. Kelley et al., Nucl. Phys. A **880** (2012) 88
 [31] C. Mahaux, P. F. Bortignon, R.A. Broglia, C. H. Dasso, Phys. Reports **120** (1985) 1
 [32] Y. Han, Y. Shi and Q. Shen, Phys. Rev. C **74** 044615 (2006)
 [33] J. Koning and J.-P. Delaroche, Nucl. Phys. A **713** (2003) 231
 [34] P.F. Bortignon, A. Bracco and R.A. Broglia, Giant resonances, Harwood Academic Publishers, Amsterdam (1998)
 [35] W.T. Pinkston and G.R. Satchler, Nucl. Phys. **72** (1965) 641
 [36] A. Bohr and B.R. Mottelson, Nuclear Structure Vol. I, Benjamin, New York (1969)

SUPPLEMENTARY MATERIAL

The mean field

The bare mean field is taken to be a Saxon-Woods potential containing a central and a spin-orbit term as in [1] (see Eq. (2-180)) :

$$U(r) = V_{WS}f(r) + V_{ls}(\vec{l} \cdot \vec{s})r_0^2 \frac{df(r)}{dr}, \quad (1)$$

with

$$f(r) = \left[1 + \exp\left(\frac{r - R_{WS}}{a_{WS}}\right) \right]^{-1}. \quad (2)$$

The k -mass has been parameterised according to,

$$m_k(r) = \mu_{red} - C_m \left[1 + \exp\left(\frac{r - R_m}{a_m}\right) \right]^{-1}, \quad (3)$$

with $a_m = 0.5$ fm, $R_m = 2.34$ fm. Far from the nucleus, the effective mass becomes equal to the reduced mass, $\mu_{red} = 10/11 = 0.91$.

The parameters of the central potential, as well as the deformation parameters β_2 and β_3 have been varied so that the solution of the Dyson equation in a box of radius $R_{box} = 40$ fm reproduces the experimental energies after renormalization (NFT)_{res} clothing). In other words, the deviation from theoretical output and experiment to be minimized is

$$\chi^2 = (\tilde{\epsilon}_{s_{1/2}} - \epsilon_{s_{1/2}}^{exp})^2 + (\tilde{\epsilon}_{p_{1/2}} - \epsilon_{p_{1/2}}^{exp})^2 + (\tilde{\epsilon}_{d_{5/2}} - \epsilon_{d_{5/2}}^{exp})^2 + (0.15 \times (\tilde{\epsilon}_{p_{3/2}} - \epsilon_{p_{3/2}}^{exp}))^2 + (0.01 \times (\beta_2 V_{WS} R_{WS} - 119))^2, \quad (4)$$

where we have also introduced the value of $\beta_2 V_{WS} R_{WS} = 119$ MeV fm derived from the experimental analysis of proton inelastic scattering used by [2] We have normalized the differences between theory and experiment, so that a similar relative error for the various quantities has a similar impact on the value of χ^2 . We have also required that the admixture of the 2^+ phonon in the wave function of the dressed $1/2^+$, $1/2^-$ and $5/2^+$ states is larger than 10%. The central term of the resulting Saxon-Woods potential and the associated effective mass are shown in Figs. 1, where they are compared with the corresponding quantities obtained from a Hartree-Fock calculation with the SGII interaction.

Calculation of the single-particle energies and spectroscopic factors

The matrix elements of the self-energy matrix $\Sigma_{i,k}(E)$ between a pair of single-particle states of ^{11}Be labeled $i \equiv \{n_i, l_i, j_i\}$, $k \equiv \{n_k, l_k, j_k\}$ and of energies $(\epsilon_i, \epsilon_k > \epsilon_F)$ is written as,

$$\Sigma_{i,k}(E) = \delta_{i,l_i} \delta_{j_i, j_k} [\delta_{n_i, n_k} \epsilon_{n_i, l_i} + \Sigma_{i,k}^{pair}(E) + \Sigma_{i,k}^{surf}(E)], \quad (5)$$

where the contribution associated with the coupling to surface vibrations is given by

$$\Sigma_{i,k}^{surf}(E) = \sum_{\lambda, n, c, \epsilon_c > \epsilon_F} \frac{h(i, c\lambda n)h(k, c\lambda n)}{E - (\epsilon_c + \hbar\omega_{\lambda n})} + \sum_{\lambda, n, c, \epsilon_c < \epsilon_F} \frac{h(i, c\lambda n)h(k, c\lambda n)}{E - (\epsilon_c - \hbar\omega_{\lambda n})} \quad (6)$$

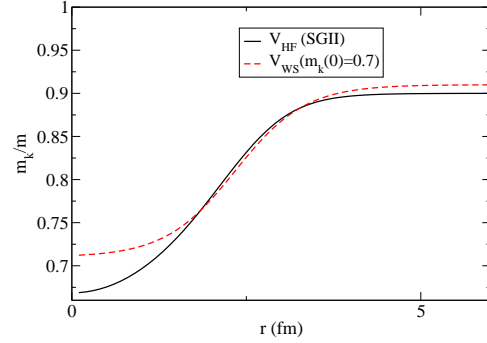
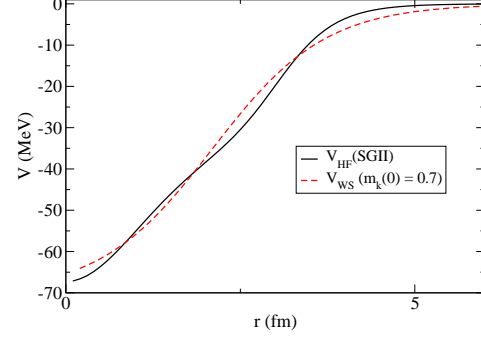


FIG. 1. The central potential (top panel) and the effective mass (bottom panel) calculated with the fitted Saxon-Woods potential are compared to the corresponding quantities obtained from a Hartree-Fock calculation with the SGII Skyrme interaction.

and that associated with the coupling to pair vibration by

$$\Sigma_{i,k}^{pair}(E) = \sum_{\lambda, n, c, \epsilon_c > \epsilon_F} \frac{h(i, c0^-)h(k, c0^{(-)})}{E + (\epsilon_c - \hbar\omega^{rem})}. \quad (7)$$

The sum is taken over the phonons λ, n and over a set of intermediate states $c \equiv \{n_c l_c j_c\}$. The matrix elements connecting single-particle level $a \equiv \{n l j\}$ with an intermediate particle-phonon state $b\lambda$ (surface), or $c0^{(-)}$ (pair) are denoted by $h(i, c\lambda n)$ and $h(i, c0^{(-)})$

We include in the calculations particle states of angular momentum $s_{1/2}, p_{1/2}$ and $d_{5/2}$ up to an energy cut off $E_{cut} = 25$ MeV. We include a single hole state, namely the $1p_{3/2}$ orbital. The self-energy matrix is diagonalized separately for each l, j , on an energy mesh, and the resulting eigenvalues $\tilde{\epsilon}_{ij}$ are a solution of the Dyson equation, $\sum_k [\Sigma_{ik}(\tilde{\epsilon}_{ij}) \times x_k^{lj}] = \tilde{\epsilon}_{ij} x_i^{lj}$.

Each solution has a single-particle component and a collective component. Denoting the eigenvectors by x_i^{lj} (normalised so that $\sum_i (x_i^{lj})^2 = 1$), the single-particle component is written as

$$\tilde{\phi}_{ij}(r) = \sum_i x_i^{lj} \phi_{n_i l_i j_i}(r), \quad (8)$$

while the collective part associated with particle-phonon configurations, $c, \lambda n$ is given by

$$\tilde{\phi}_{\lambda,n,l,c}^{coll}(r) = \sum_{n_c} R_{(c,\lambda n)_{lj}}^{coll} \phi_{n_c,l,c}(r), \quad (9)$$

where $R_{(c,\lambda n)_{lj}}^{coll} = \sum_i x_i^{lj} \frac{h(i,c,\lambda n)}{E - (\epsilon_c + \hbar\omega_{\lambda,n})}$ for $\epsilon_c > \epsilon_F$ and $R_{(c,\lambda n)_{lj}}^{coll} = \sum_i x_i^{lj} \frac{h(i,c,\lambda n)}{E - (\epsilon_c - \hbar\omega_{\lambda,n})}$ for $\epsilon_c < \epsilon_F$. The square of the single particle component of the dressed state is then given by

$$a_{ij}^2 = \frac{1}{1 + \sum_{c,\lambda,n} (R_{(c,\lambda n)_{lj}}^{coll})^2} \quad (10)$$

while the admixture of the solution with the $c, \lambda n$ configuration is given by

$$a_{(c,\lambda n)_{lj}}^2 = \frac{(R_{(c,\lambda n)_{lj}}^{coll})^2}{1 + \sum_{c,\lambda,n} (R_{(c,\lambda n)_{lj}}^{coll})^2} \quad (11)$$

The above solution provides the first term of the series of rainbow diagrams dressing the single-particle states, taking into account the effect of many-phonon configurations. Higher order terms can be generated iterating the solution self-consistently [3]. We have not attempted to perform such a calculation in the present paper, but employ empirical renormalisation, choosing the single-particle intermediate states so as to reproduce the (low-lying) experimental energies, and eventually the outcome of the clothing process, i.e. $\tilde{\epsilon}_{ij}$ and $\tilde{\phi}_{ij}$. In other words, the solution of the Dyson equation will be acceptable only if the single-particle component of the solution is in agreement with the input used for the intermediate basis, a requirement imposing a severe self-consistent condition to our diagonalization process. In the calculations we have added a correction to the energy of the intermediate particle-phonon configurations, to correct for Pauli principle violation associated with many-phonon states (anharmonicities, see Fig. 1(IV) of the main text), implicitly considered in the empirical renormalization. Such corrections are particularly important in the case of the renormalization of the $d_{5/2}$ states, because of the conspicuous coupling to the $s_{1/2} \otimes 2^+$ configuration.

The $2s_{1/2}$ orbital is not bound in our initial bare potential. As a consequence, if we use the same basis for the asymptotic and the intermediate states, the coupling matrix element will be small due to the poor overlap in the corresponding radial wavefunctions. Iterating the diagonalization, the $s_{1/2}$ state eventually becomes bound, acquiring in the process a collective component of the type $d_{5/2} \otimes 2^+$. At the same time, $5/2^+$ states will acquire both a bound collective component through the coupling with the $s_{1/2} \otimes 2^+$ configuration and a localized (resonant) single-particle wave function due to the mixing of the various continuum states. For economy, these processes are taken into account within the framework of empirical renormalization using a (intermediate) $s_{1/2}$ state bound by 0.5 MeV as in experiment, and verifying that this value coincides with the energy $\tilde{\epsilon}_{1/2^+}$ of the final dressed $|1/2^+ \rangle$ state.

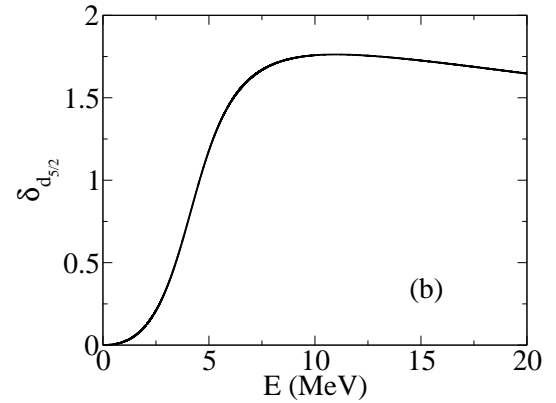
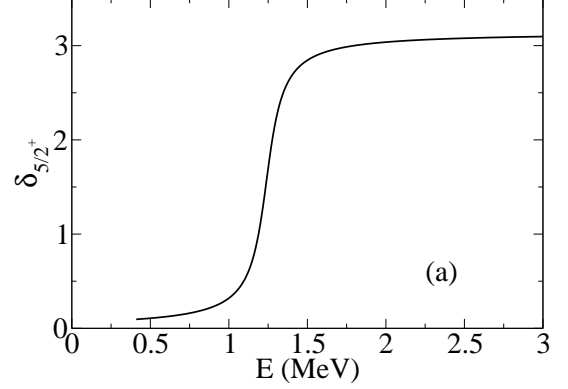


FIG. 2. (a) $5/2^+$ (NFT) $_{ren}$ phase shifts as a function of energy. (b) $d_{5/2}$ phase shifts calculated with the bare potential.

The renormalised $5/2^+$ phase shift, displaying a resonance at $E_{res} = 1.23$ MeV of width $\Gamma = 160$ keV, are shown in Fig. 2, where they are compared with the phase shifts calculated with the bare potential, displaying a broad resonance at $E = 6.5$ MeV.

Bubble overcounting

Freely summing over intermediate particle \otimes phonon configurations when evaluating the self-energy diagrams, leads as a rule to some overcounting, since phonons are linear combinations of particle-hole configurations (see Fig.3)

Such overcounting can be cured subtracting the overcounted bubble diagram from the particle-phonon (RPA series) calculation. In the present case, such overcounting is small (a few per cent, smaller than our global theoretical accuracy). In fact, the low lying 2^+ phonon, which is by far the most relevant phonon in our calculations, is constructed mostly out of particle-hole transitions between single-particle states of negative parity ($1p_{3/2}^{-1}$ holes; $p_{1/2}$ (mainly), $p_{3/2}$ (very little), $f_{7/2}$ and $f_{5/2}$ (negligibly) particles) and marginally by particle-hole transitions of positive parity ($1s_{1/2}^{-1}$ holes, $d_{5/2}$ and $d_{3/2}$ particles). As a consequence, when evaluating the

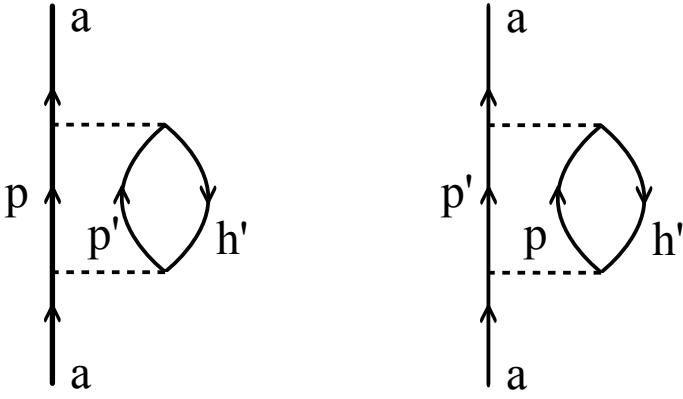


FIG. 3. The diagram at the right contains the same intermediate configuration as that of the left one. If antisymmetrised two-body matrix elements are used, these two diagrams are identical.

(positive parity) self-energies of the $s_{1/2}$ and $d_{5/2}$ states, the intermediate $p \otimes 2^+$ configuration involves particle states of positive parity, and overcounting is produced only by the small positive parity particle-hole components of the 2^+ phonon (see Figs. 4). On the other hand when evaluating the (negative parity) $p_{1/2}$ self-energy no overcounting arises since only one $p_{3/2}$ hole contributes and no involved summation can lead to overcounting (see Figs. 4).

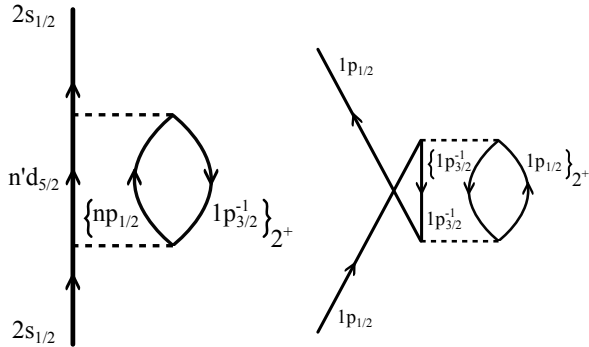


FIG. 4. (left) Main p'-h' configuration renormalizing the $2s_{1/2}$ state. Summing over the number of nodes n and n' does not lead to double counting, in keeping with the different parity and angular momentum of the $d_{5/2}$ and $p_{1/2}$ states. An identical reasoning applies to the $5/2^+$ states. (right) Main p'-h' configuration renormalizing the $2p_{1/2}$ state. In this case only the $1p_{3/2}^{-1}$ hole state is taken into account, and no overcounting is possible.

Anharmonic effects

An important point concerns anharmonic effects in many-phonon configurations, associated with the Pauli principle, which are not taken into account in the rainbow series. They are particularly relevant in the present case due to the low angular moment of the single-particle states involved in the calculation. The intermediate configurations $\tilde{d}_{5/2} \otimes 2^+$ and

$\tilde{s}_{1/2} \otimes 2^+$ implicitly contain a 2-phonon component and this involves an anharmonic effect associated with violation of the Pauli principle. In NFT the Pauli principle is restored by the so called butterfly diagram (and associated ones, see [4], Eqs. (28-35)), which takes into account the fermion exchange between the microscopic p-h structures of the involved phonons. We have not calculated in detail the diagram but we have estimated the associated correction by performing a RPA calculation blocking the relevant p-h transitions. This is an approximate method which coincides with the exact evaluation of the butterfly diagram in the two-level model. We obtain an increase of the energy of the two-phonon configuration of 2.7 MeV and a reduction of the deformation β_2 parameter of about 30%. The influence of these changes on the empirical-particle-phonon configurations energy depends on how much two-phonon weight they carry, which in turn is an output of our calculations. A consistent calculation leads to an increase of 2.4 MeV for the $d_{5/2} \otimes 2^+$ configuration and of 1.2 MeV for the $s_{1/2} \otimes 2^+$ one. The difference between these two corrections reflects the fact that the calculated 2^+ phonon admixture in the dressed $5/2^+$ state (50%) is about twice the value obtained for the $1/2^+$ state (20%). The $\tilde{d}_{5/2} \otimes 2^+$ and $\tilde{s}_{1/2} \otimes 2^+$ configurations corrected for the Pauli principle are those entering diagrams (I)(a) and (III)(a) and (b) of Fig. 1 of the main text (see Fig. (IV) for the corresponding corrections).

Calculation of the dipole matrix element

The measured value of the transition strength associated with the dipole transition between the first excited state and the ground state of ^{11}Be is $B(E1) = 0.102 \pm 0.02 \text{ e}^2 \text{ fm}^2 = 0.32 \text{ W.U.}$ [5] ($1 \text{ W.U.} = 1/4\pi(3/4)^2(1.2A^{1/3})^2 = 0.3188 \text{ e}^2 \text{ fm}^2$). The transition strength is defined as

$$B(E1; I_i \rightarrow I_f) = \frac{1}{2I_i + 1} | \langle I_f || iM(E1) || I_i \rangle |^2 \quad (12)$$

The leading contribution for the $1/2^+ \rightarrow 1/2^-$ transition is obtained calculating the transition between the single-particle part of the renormalised wave functions, weighted with the appropriate single-particle factor and multiplied by the recoil effective charge $e_{eff} = -eZ/A = -4e/11$:

$$B(E1; I_i \rightarrow I_f) = \frac{e_{eff}^2}{2I_i + 1} a_{1/2^+}^2 a_{1/2^-}^2 |M^0|^2 \quad (13)$$

where

$$M^0 \equiv \langle 1/2^- || iM(E1) || 1/2^+ \rangle = \sqrt{\frac{3}{2\pi}} \frac{-1}{\sqrt{3}} I(E1) = -\sqrt{\frac{1}{2\pi}} I(E1), \quad (14)$$

with $I(E1) = \int dr \tilde{\psi}_{1/2^+}(r) r \tilde{\psi}_{1/2^-}(r)$. The amplitudes are equal to $a_{1/2^+}^2 = 0.83$ and $a_{1/2^-}^2 = 0.81$ (Figs. 1 of the main text, Eqs.(1) and (2), upper box) Numerically we find $I(E1) \approx 5 \text{ fm}$, and then obtain the zero-order result

$$B(E1; 1/2^+ \rightarrow 1/2^-) \approx \frac{16}{121} \frac{1}{2} 0.67 \frac{1}{2\pi} 25 \text{ e}^2 \text{ fm}^2 = 0.17 \text{ e}^2 \text{ fm}^2. \quad (15)$$

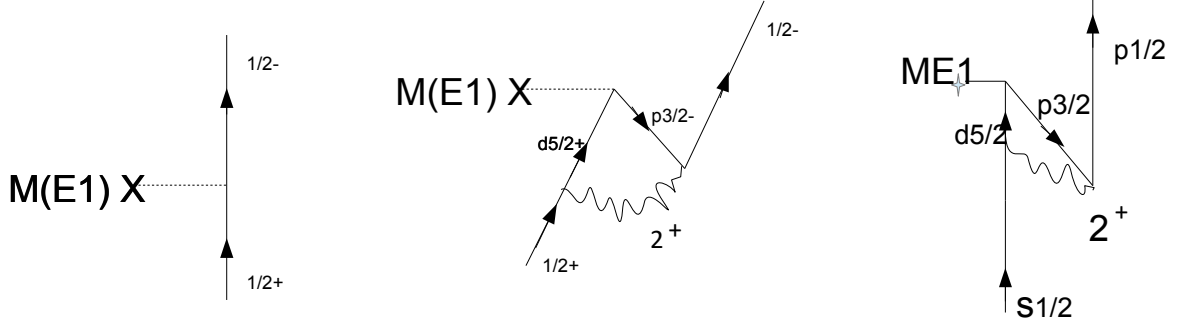


FIG. 5. Main processes contributing to the dipole transition between the first excited state and the ground state of ^{11}Be . The vertex correction associated with the low-lying 1^- strength (incipient GDR) is estimated to be small.

One has to consider, however, that one expects other important contributions from many-body processes. The two time orderings associated with the most important ones are shown in the right part of Figs. 5. They interfere in a destructive way with the leading contribution, leading to

$$B(E1; I_i \rightarrow I_f) = \frac{e_{eff}^2}{2I_i + 1} a_{1/2^+}^2 a_{1/2^-}^2 |M^0 + M^{1(a)} + M^{1(b)}|^2 = \frac{16}{121} \frac{1}{2} 0.66 \left| \sqrt{\frac{1}{2\pi}} \times 5 - 0.25 - 0.19 \right|^2 e^2 \text{fm}^2 = 0.11 e^2 \text{fm}^2. \quad (16)$$

We remark that the usual depletion of the low-lying E1 strength by the giant resonance is not very effective in the present case, due to the poor overlap between the halo neutron single-particle states and those of the nucleons of the core (see [6],[7] p.2 and App. A,B; see also [8]). In fact, it can be estimated that the contribution of the giant dipole polarisation diagram is much smaller than the bare M(E1) diagram due to the halo character of the wave functions, and that it also much smaller than the second order quadrupole polarisation corrections due to the smaller deformation parameter of the GDR compared to quadrupole mode, and to its much larger excitation energy.

Calculation of the charge radius

An estimate of the difference between the value of the charge radius in ^{11}Be and ^{10}Be can be obtained by considering that the dressed $1/2^+$ wave function has a $s_{1/2}$ single-particle part with amplitude $a_{1/2^+} = \sqrt{0.83}$ and a collective part dominated by the admixture with the lowest 2^+ vibration of amplitude $a_{(d_{5/2^+} \otimes 2^+)_{1/2^+}} = \sqrt{0.17}$. The contribution to the square charge radius due to the single-particle part is due to core recoil:

$$(a_{1/2^+})^2 \left(\langle r^2 \rangle_{^{10}\text{Be}} + \left(\frac{\langle r^2 \rangle_{s_{1/2}}^{1/2}}{11} \right)^2 \right) \quad (17)$$

The contribution of the collective part is instead given by

$$a_{(d_{5/2^+} \otimes 2^+)_{1/2^+}}^2 \left(\langle r^2 \rangle_{^{10}\text{Be}} \left(1 + \frac{2}{4\pi} \beta^2 \right) + \left(\frac{\langle r^2 \rangle_{d_{5/2, \text{coll}}}^{1/2}}{11} \right)^2 \right), \quad (18)$$

where we have used the fact that the radius of the nucleus in its 2^+ state (first excited state of a harmonic oscillator) is a factor $(1 + \frac{2}{4\pi} \beta^2)$ larger than in its ground state, while the neutron in the $(d_{5/2^+} \otimes 2^+)_{1/2^+}$ state is described by the wave function $\psi_{d_{5/2, \text{coll}}}$. One then obtains

$$\langle r^2 \rangle_{^{11}\text{Be}} = \langle r^2 \rangle_{^{10}\text{Be}} + (a_{1/2^+})^2 \left(\frac{\langle r^2 \rangle_{s_{1/2}}^{1/2}}{11} \right)^2 + a_{(d_{5/2^+} \otimes 2^+)_{1/2^+}}^2 \left(\langle r^2 \rangle_{^{10}\text{Be}} \frac{2\beta^2}{4\pi} + \left(\frac{\langle r^2 \rangle_{d_{5/2, \text{coll}}}^{1/2}}{11} \right)^2 \right). \quad (19)$$

Introducing the values $\langle r^2 \rangle_{^{10}\text{Be}} = 5.57 \text{ fm}^2$, $(a_{1/2^+})^2 = 0.83$, $a_{(d_{5/2^+} \otimes 2^+)_{1/2^+}}^2 = 0.17$, $\beta_2 = 1.2$, $\langle r^2 \rangle_{s_{1/2}}^{1/2} = 7.1 \text{ fm}$ and $\langle r^2 \rangle_{d_{5/2, \text{coll}}}^{1/2} = 3 \text{ fm}$ one obtains $\langle r^2 \rangle_{^{11}\text{Be}} = 5.57 + 0.83 \times 0.42 + 0.17 \times (1.27 + 0.07) = 6.15 \text{ fm}^2$, and $(\langle r^2 \rangle_{^{10}\text{Be}})^{1/2} = 2.48 \text{ fm}$, to be compared with the experimental value $2.46 \text{ fm} \pm 0.015$ [9].

Coupled equations

An approximate solution of the Schrödinger equation $H\Psi_a = E\Psi_a$ for the wave function of the clothed odd nucleon can be expressed as

$$\Psi_a = [\tilde{\phi}_{l_a j_a} + [\tilde{\phi}_{l_b j_b \lambda}^{\text{coll}} \cdot \Gamma_\lambda^\dagger]_{j_a} - \tilde{\phi}_{l_a j_a} - [\tilde{\phi}_{l_c j_c \lambda}^D \cdot \Gamma_\lambda]_{j_a}] \Phi_{GS}^A \quad (20)$$

where Φ_{GS}^A denotes the ground state of the nucleus of even mass number A (containing the correlations needed so that it is the vacuum of the different elementary modes of excitation used as a basis to describe ^{11}Be (i.e. $a_j |\Phi_{GS}^A\rangle = \Gamma_{n\lambda} |\Phi_{GS}^A\rangle = 0$), Γ_λ^\dagger denotes a general creation operator of a vibrational state (phonon), calculated using e.g. RPA,

$$\tilde{\phi}_{l_a j_a} = R^x / r_{l_a j_a} \Theta_{l_a j_a} \quad (21)$$

creates a particle in l_a, j_a ,

$$[\tilde{\phi}_{l_b j_b \lambda}^{coll} \cdot \Gamma_{\lambda}^{\dagger}]_{j_a} = (R_{b\lambda}^C(r)/r) [\Theta_{j_b} \cdot \Gamma_{\lambda}^{\dagger}]_{j_a} \quad (22)$$

creates a particle-phonon state coupled to j_a and parity $(-1)^{l_a}$,

$$\bar{\phi}_{l_a j_a} = (R_{l_a j_a}^y / r) \Theta_{l_a j_a} \quad (23)$$

annihilates a hole in l_a, j_a and

$$[\bar{\phi}_{l_c j_c \lambda} \cdot \Gamma_{\lambda}]_{j_a} = (R_{c\lambda}^D(r)/r) [\Theta_{j_c} \cdot \Gamma_{\lambda}]_{j_a}, \quad (24)$$

annihilates a hole-phonon coupled to j_a and parity $(-1)^{l_a}$, where the radial wavefunctions R_a^x and $R_{b\lambda}^C$ must be expanded over a set of single-particle states (HF) lying above the Fermi energy:

$$R_a^x(r) = \sum_i x^{a_i} R_{a_i}^{HF}(r) \quad , \quad R_{b\lambda}^C(r) = \sum_i R_{b_i \lambda}^{coll} R_{b_i}^{HF}(r); \epsilon_{a_i}, \epsilon_{b_i} > \epsilon_F \quad (25)$$

while R_a^y and $R_{c\lambda}^D$ must be expanded over the occupied states:

$$R_a^y(r) = \sum_i y^{a_i} R_{a_i}^{HF}(r) \quad , \quad R_{c\lambda}^D(r) = \sum_i R_{c_i \lambda}^{coll} R_{c_i}^{HF}(r); \epsilon_{a_i}, \epsilon_{c_i} < \epsilon_F. \quad (26)$$

The radial wave function $R_{c\lambda}^D(r)$ accounts for the proper antisymmetrization of the RPA ground state. In fact the RPA ground state contains 2p-2h configurations, what implies that the odd particle will find states inhibited by the Pauli principle also above ϵ_F . Reciprocally the R^y wave accounts for the possibility that the impinging particle will find available states below ϵ_F .

It can be shown that the radial wave functions satisfy the coupled equations

$$\left[-\frac{\hbar^2}{2m} \frac{\partial^2}{\partial r^2} + V_a(r) + 0\hbar\omega \right] R_a^x(r) + \Xi_{a,b\lambda}(-rdV/dr) R_{b\lambda}^C(r) - \Xi_{a,c\lambda}(-rdV/dr) R_{c\lambda}^D(r) = ER_a^x(r)$$

$$\Xi_{a,b\lambda}(-rdV/dr) R_a^x(r) + \left[-\frac{\hbar^2}{2m} \frac{\partial^2}{\partial r^2} + V_b(r) + 1\hbar\omega \right] R_{b\lambda}^C(r) - \Xi_{a,b\lambda}(-rdV/dr) R_a^y(r) = ER_{b\lambda}^C(r)$$

$$\Xi_{a,b\lambda}(-rdV/dr) R_{b\lambda}^C(r) - \left[-\frac{\hbar^2}{2m} \frac{\partial^2}{\partial r^2} + V_a(r) + 0\hbar\omega \right] R_a^y(r) + \Xi_{a,c\lambda}(-rdV/dr) R_{c\lambda}^D(r) = -ER_a^y(r)$$

$$\Xi_{a,c\lambda}(-rdV/dr) R_a^x(r) - \left[-\frac{\hbar^2}{2m} \frac{\partial^2}{\partial r^2} + V_c(r) - 1\hbar\omega \right] R_{c\lambda}^D(r) + \Xi_{a,c\lambda}(-rdV/dr) R_a^y(r) = -ER_{c\lambda}^D(r) \quad (27)$$

where

$$V_a(r) = V(r) + V_{ls}(r) + V_{cent}(r) \quad (28)$$

and

$$\Xi_{a,b\lambda} = \langle \Theta_{j_a m_a} \sum_{\lambda\mu} \beta_{\lambda} Y_{\lambda\mu} [\Gamma_{\lambda\mu}^{\dagger} + (-1)^{\mu} \Gamma_{\lambda\mu}] [\Theta_{j_b} \cdot \Phi_{\lambda}]_{j_a m_a} \rangle \quad (29)$$

The conditions (25) and (26) imply that these equations must be solved using projection techniques.

Calculation of the absolute differential cross sections

The calculations of the angular distribution of the reaction $^{10}\text{Be}(d,p)^{11}\text{Be}(J_f^{\pi})$ have been performed in the post representation for the final bound states $J_f^{\pi} = 1/2^+$ and $1/2^-$ while the prior representation has been adopted for the unbound state $5/2^+$, to ensure a rapid convergence. The transfer form factor is obtained from the single-particle component of the many-body wave function. In the case of the $5/2^+$ final state, the $^{10}\text{Be}-n$ potential $V_{10\text{Be}-n}$ is also required. We have approximated $V_{10\text{Be}-n}$ with the bare Saxon-Woods potential of increased depth (bringing it to $V_{WS} = -90$ MeV), so that the associated $d_{5/2}$ elastic phase shift displays a resonance for $E \approx 1.20$ MeV. The angular distribution is obtained by summing the cross sections associated with each of the $5/2^+$ eigenstates calculated in a given box and lying in the region of the resonance (discretized continuum). Convergence is obtained for boxes of the order of 40 fm. We note that the cross section associated with each individual peak of energy E_n approximately represents the value of the cross section integrated over an energy interval lying between $(E_{n-1} + E_n)/2$ and $(E_n + E_{n+1})/2$. In order to compute the energy distribution

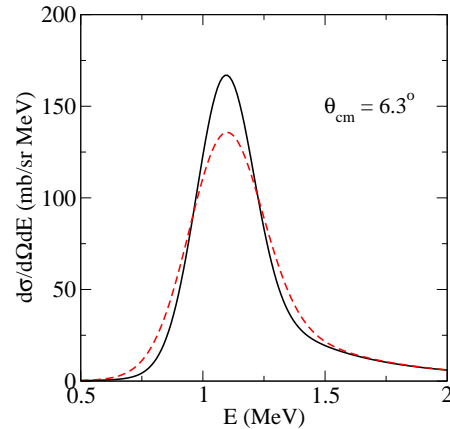


FIG. 6. The theoretical absolute double differential cross section calculated for the reaction $^{10}\text{Be}(d,p)^{11}\text{Be}$ populating the $5/2^+$ state at $\theta_{cm} = 6.3^\circ$ is shown by the solid line. The dashed line shows the result of convoluting this curve with a Gaussian curve of FWHM = 220 keV (estimated experimental resolution).

$d^2\sigma/dEd\Omega$ for a given value of θ on a sufficiently fine energy mesh, we have adopted a continuum energy distribution with a Voigt shape, fitting the parameters so that the integrals of the distribution best reproduce the values obtained in the different boxes in the appropriate intervals. We have folded the theoretical calculation with a gaussian curve of $FWHM = 220$ keV, representing the experimental resolution, estimated from the width of the peaks of the discrete states (cf. Fig. 6). We note that the experimental cross sections contain a background caused by the other partial waves, that we have not considered in our present calculation. Finally, we have also calculated the angular distribution associated with the one-nucleon transfer reaction $^{11}\text{Be}(p,d)^{10}\text{Be}$ populating the 2^+ state in ^{10}Be in the post representation, making use of the collective part $R_{d_{5/2,2^+}}^C$

of the initial $1/2^+$ state in ^{11}Be (see Sect. 4).

- [1] A. Bohr and B.R. Mottelson, *Nuclear Structure Vol. I*, Benjamin, New York (1969)
- [2] H. Iwasaki *et al.*, *Phys.Lett.* **B481**, 7 (2000)
- [3] A. Idini, F. Barranco and E. Vigezzi, *Phys. Rev.* **C 85** (2012) 014331
- [4] D.R. Bes, R.A. Broglia, G.G. Dussel, R.J. Lotta and H.M. Sofia, *Nucl. Phys. A* **260** (1976) 1
- [5] E. Kwan *et al.*, *Phys. Lett.* **B732** (2014) 210
- [6] F. Barranco, P.F. Bortignon, R.A. Broglia, G. Colò and E. Vigezzi, *Eur. Phys. J. A* **11**, 385 (2001)
- [7] R.A. Broglia, P.F. Bortignon, F. Barranco, E. Vigezzi, A. Idini and G. Potel, *Phys. Scr.* **91** (2016) 063012
- [8] I. Hamamoto and S. Shimoura, *J. Phys.* **G34** (2007) 2715
- [9] A. Krieger *et al.*, *Phys. Rev. Lett.* **108** (2012) 142501